Journal of Nano- and Electronic Physics
Vol. **13** No 6, 06023(7pp) (2021)

Журнал нано- та електронної фізики
Том **13** № 6, 06023(7cc) (2021)

Iron-Doped Titania: Synthesis, Structural, Magnetic and Photocatalytic Properties

Ivan Mironyuk[1], Volodymyr Kotsyubynsky[1,*], Igor Mykytyn[1], Yulia Kotsyubynska[2], Volodymyra Boychuk[1], Vasyl Fedoriv[1]

[1] *Vasyl Stefanyk Precarpathian National University, 57, Shevchenko St., 76018 Ivano-Frankivsk, Ukraine*
[2] *Ivano-Frankivsk National Medical University, 2, Halytska St., 76018 Ivano-Frankivsk, Ukraine*

(Received 25 May 2021; revised manuscript received 09 December 2021; published online 20 December 2021)

Ultrafine Fe-doped TiO_2 (Fe content of 0, 0.5, 2, 5, 10, and 20 wt. %) was prepared using two-stage $TiCl_4$ and $FeCl_3{\cdot}6H_2O$ hydrolysis at final pH = 3.5. The effect of the Fe ion weight concentration on the phase composition and morphology was investigated using XRD, FTIR, Mossbauer spectroscopy, thermal analysis, and low-temperature nitrogen adsorption. Increasing the content of Fe^{3+} ions in the range of 0-10 wt. % causes an increase in the amount of the anatase phase from 0 to 85-90 %. The average size of anatase particles decreases from 31 nm for a Fe content of 0.5 wt. % to about 4 nm for a Fe content of 10 wt. %. The material synthesized at an Fe ion concentration of 20 wt. % is amorphous (XRD data) without any magnetically ordered iron-containing phase. The Mossbauer spectra of all Fe-doped TiO_2 samples consist of doublets only, with isomer shift values of 0.55-0.57 mm/s corresponding to Fe^{3+} in a high-spin state in octahedral coordination, so isomorphic substitution of Ti^{4+} ions for Fe^{3+} is highly probable. Annealing of Fe-doped TiO_2 sample with a maximum doping degree (20 wt. %) at 900 °C leads to the formation of the Fe_2TiO_5 pseudobrookite phase and the transition of amorphous anatase to monoclinic titania (space group symmetry C12/m1). The BET specific surface area values of Fe-doped titania increase linearly from 70 to 350 m^2/g with increasing iron content from 0 to 5 wt. %. Further increase in the iron content does not affect the BET surface area. The growth of oxygen vacancies concentration with increasing Fe^{3+} content was observed by FTIR that corresponds to the reduction of the rutile lattice constant. The anatase-rutile transition temperature (thermal analysis data) is the highest (about 575 °C) for the material with the maximum Fe ion content. Photocatalytic activity of Fe-doped TiO_2 samples in reaction of methylene blue degradation increases with an increase in the Fe content and correlates with the anatase phase relative concentration. The reaction rate increases from about 0.008 to 0.028 min^{-1}, while the reaction rate for commercial photocatalyst Degussa P25 under the same experimental conditions is about 0.029 min^{-1}.

Keywords: Fe-doped titania, Hydrolysis, Polycondensation, Nucleation, Titania.

DOI: 10.21272/jnep.13(6).06023 PACS numbers: 42.62.Fi, 42.70.Qs, 61.66.Fn

1. INTRODUCTION

Nanocrystalline titania has a wide range of applications as photocatalysts [1], sensors [2], electrode materials for electrochemical [3] or photovoltaic [4] devices. Phase composition, particle size and surface state are the most important characteristics which determine catalytic reactivity, photosensitivity and adsorption properties of TiO_2 [5].

A promising way of obtaining new functional nanomaterials is the synthesis of nanocomposite systems (isolated nanoclusters incorporated in a porous matrix, or combined compounds with isomorphic substitution of dopant ions in the matrix of the crystal structure of the base material) [6]. The doping makes it possible to improve the photocatalytic, electrochemical and photoelectrochemical properties of TiO_2. Titania doping with metal ions shifts the absorption spectra to the visible region, increases electrical conductivity and increases the performance of photovoltaic devices [7]. The ionic radius of Fe^{3+} (0.64 Å) is close to that of Ti^{4+} (0.68 Å), therefore, isomorphous substitution during liquid phase synthesis is possible. An increase in the photocatalytic activity of Fe-doped titania was reported by some authors, see for example [8, 9]. The most possible reasons are the capture of charge carriers by Fe^{3+} ions substituted in the TiO_2 matrix and suppression of the recombination of photogenerated electron-hole pairs. Phase composition and particle size control are crucially important for enhancing the photocatalytic response of Fe-containing titania. Anatase modification of TiO_2 due to electronic structure peculiarities (indirect band gap transition) has advantages compared to other polymorphic forms (rutile and brookite) [10], but in some cases the presence of interphase boundaries within titania particles is very important for catalytic activity growth. In this paper, the development of methods of active influence on the phase composition of iron doped TiO_2 is reported.

2. MATERIALS AND METHODS

A sol-gel method based on the preparation of titanium tetrachloride during hydrolysis was used for the synthesis of ultrafine $FeTiO_2$ [11]. Titanium tetrachloride $TiCl_4$ (Merck, 99.9 %; specific density 1.73 g/cm^3 at 20 °C) was cooled to 0 °C. Hydrochloric acid (36.0 % aqueous solution) was added to titanium tetrachloride at a stabilized temperature with the evaporation of gaseous hydrogen chloride and the formation of titanium oxychloride $TiCl_3OH$ sol. The final $TiCl_4$:hydrochloric acid volume ratio was 2:1 and the pH value was 3.5. An aqueous solution of ferric chloride hexahydrate $FeCl_3{\cdot}6H_2O$ (Merck, reagent grade, ≥ 98 %) in the ratios required to obtain the predicted mass concentration of Fe was added dropwise at vigorous stirring. The result-

* kotsuybynsky@gmail.com

ing sol was transparent and had a yellowish tinge. An aqueous solution of sodium hydrocarbonate was added dropwise to the sol to pH = 5.0-5.5 under vigorous stirring. Gel formation was observed during the entire process of increasing pH. The suspension of nanoparticles was kept at 80 °C for 4-5 h, followed by washing with distilled water until the absence of Na^+ and Cl^- ions. Precipitated TiO_2 was dried at a temperature of 120 °C. Six samples with different Fe contents of 0, 0.5, 2, 5, 10 and 20 wt.% were obtained, designated 0.5Fe, 2Fe, 5Fe, 10Fe and 20Fe, respectively.

XRD patterns were obtained on a DRON-4-07 diffractometer (CuK_α radiation, Bragg-Brentano geometry type, Ni K_β-filter). Full pattern Rietveld refinement was done using FullProf Suite Program [12]. The structural models for anatase and rutile were based on ICSD #92363 [13] and ICSD #24780 [14], respectively. A combination of Gauss and Cauchy functions was used to fit the diffraction lines. The size of the coherent scattering domains was calculated by the Scherrer equation: $D = K\lambda/(\beta\cos\theta)$, where K is the Scherrer constant ($K = 0.9$), λ is the wavelength (0.15405 nm), β is the FWHM (in radians), and θ is the peak angular position. Copper powder annealed in vacuum (850-900 °C, 4 h) with an average grain size of about 50 μm was used as a reference sample to determine the instrumental peak broadening. The full width at half maximum (FWHM) of the diffraction peak of this reference sample at $2\theta = 43.38°$ was 0.129°, therefore it made it possible to distinguish anatase and brookite phases.

Infrared spectra were obtained on a Thermo-Nicolet Nexus 670 FTIR spectrometer in a range of 4000-400 cm^{-1}. The TiO_2 / K Br mixture after vibration milling was pressed into pellets and measured in the transmission mode.

Mossbauer spectra were obtained on a MS1104Em spectrometer with moving absorber ($^{57}Co(Cr)$ radiation source, isomer shift calibrated according to α-Fe). The velocity resolution was about 0.008 mm/s per channel. The obtained signal-to-noise ratios were higher than 31. The Mossbauer spectra were measured at room temperature in transmission geometry.

The values of specific surface area of the obtained materials (five-point BET method) were measured by low-temperature nitrogen adsorption/desorption at 77 K with a Quantachrome NOVA 2200e device.

The photocatalytic activity of the obtained Fe-doped titania was investigated by methylene blue (MB) decolorization in an aqueous solution (mass concentration of 0.01 g/l) under soft UV irradiation (27 W, mainly with a wavelength of 365 nm). Dry titania powder (mass concentration 0.1 g/l) after continuous grinding was added into aqueous solution of MB. The total volume of reaction media was 50 ml, interface area 30 cm^2, the irradiation under magnetic stirring. The reaction time ranged from 0 to 50 min, the measurements of the concentration was performed each 10 min. The titania and solution were separated with centrifuge. The changes of reaction media absorbance were measured with UV/Vis spectrophotometer Ulab 108UV, China.

3. RESULTS AND DISCUSSION

An increase in the iron-containing precursor in the reaction medium abruptly affects the phase state of the obtained materials (Fig. 1a). The material obtained in the absence of Fe additive (Fe^0) is a pure rutile phase with an average size of the coherent scattering domains (particles) of about 4.7 nm. An increase in the Fe^{3+} ion content leads to the appearance and gradual growth of anatase phase molar content. The crystallinity of both titania phases decreases with increasing Fe ion content and sample with maximal doping degree is amorphous. Iron-containing phases were not observed for all synthesized samples. For 0.5Fe sample with anatase content up to 4 mol. % the average size of anatase particles is larger (about 31 nm) compared to the rutile phase (about 4 nm), but already for 2Fe sample (anatase content of about 45-50 mol. %) this value is about 4.9 nm. The tendency to an increase in the rutile phase particle size is observed up to Fe contents of 2 wt. % that corresponds to an increase in both lattice constants (Fig. 1c). An increase in the doping degree causes a fast decline of titania particle size for the rutile and anatase phases (up to 2.2 and 3.8 nm, respectively). A nearly linear enlargement of the specific surface area of Fe-doped titania in the range 70-350 m^2/g was observed up to an iron content of 5 wt. % with subsequent stabilization (Fig. 2).

The doping degree enlargement causes an increase in the thermodynamic instability of the oxide system with relaxation through phase and structural transformations. The dependence of the Fe-containing titania phase composition on the content of iron ions was studied earlier in several works. Brookite and Fe-containing phases were observed in [15] for hydrothermally synthesized Fe-TiO_2 (Fe content in a range of 0-30 wt. %). It is known that the synthesis conditions

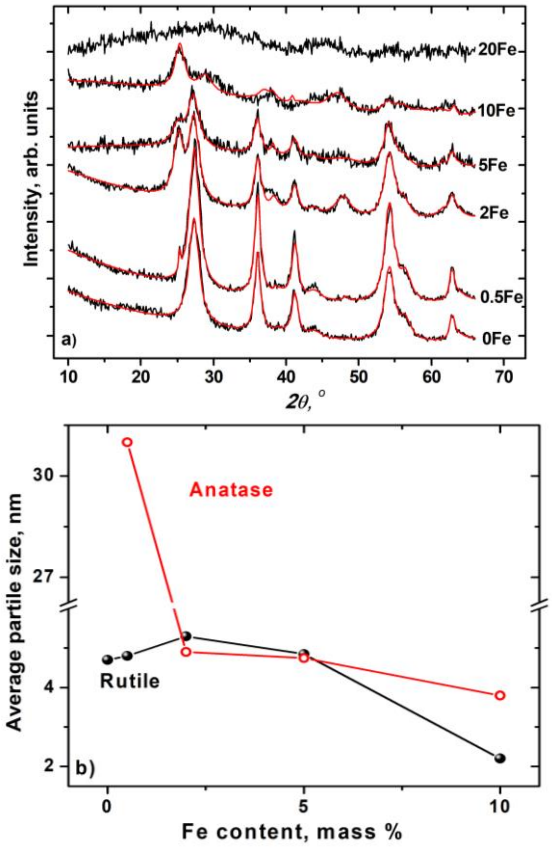

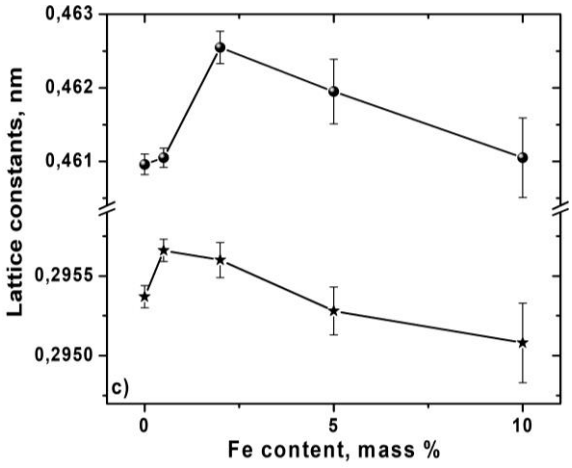

Fig. 1 – XRD patterns of Fe-doped TiO_2 samples (a), changes in the average particle size (b) and the rutile phase lattice constant (c) as a function of Fe content

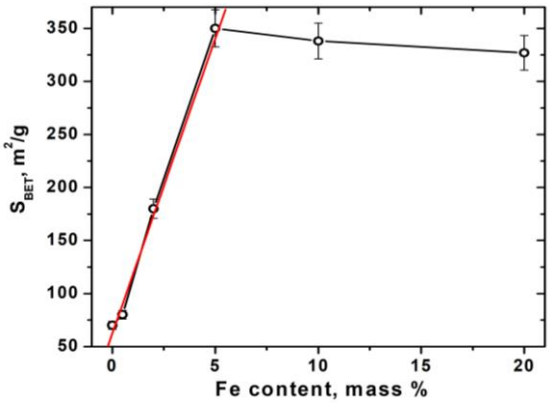

Fig. 2 – BET specific surface area of Fe-doped TiO_2 samples vs Fe content

(especially the pH value of the reaction media [11] and the presence of different additives [16-18]) affect the nucleation of titania phases. An increase in the anatase-rutile phase transition rate in the presence of Cu^{2+} ions in a reducing atmosphere was interpreted in [19] as a result of anion vacancies formation, but this factor is less important than the effect of morphology change.

A decrease in the titania particle sizes with a simultaneous increase in the anatase phase formation with Fe content enlargement in a range of 1-15 wt. % was observed in [20]. A decrease in the number of titania particles with increasing Fe/Ti ratio is typical of Fe-doped TiO_2 [21, 22]. The probability of rutile nucleation at a given temperature depends on the ratio between the phase transition energy (calculated as the difference between the Gibbs energies of anatase and rutile particle sizes) and the energy of the interface between the nuclei of a new phase (rutile) and the matrix phase (anatase). The surface energy values for {001}, {101} and {010} facets of anatase are 0.90, 0.44 and 0.53 J/m^2, respectively [23], while for rutile these values are much higher – about 2.2 ± 0.2 J/m^2[24]. As a result, the anatase-rutile transition probability decreases with decreasing anatase crystallite size.

FTIR spectroscopy provides additional information about the obtained materials. A characteristic feature of the IR spectra of $TiO_2 \cdot H_2O$ material is broad absorption bands at about 1630 and 3200 cm^{-1}, corresponding to the vibrational modes of OH bonds of adsorbed non-dissociated H_2O molecules (δ-H_2O) and chemisorbed hydroxyl groups (ν-OH), respectively [25, 26]. The considerable width of the absorption bands of OH bonds (3000-3750 cm^{-1}) indicates the presence of continuous spectra of resonant energies. The blue shift of the absorption maximum with increasing doping degree corresponds to length reduction of OH bonds.

The zone of very strong absorption at the beginning of the investigated wavelength region corresponds to Ti–O and Ti–O–Ti vibrations of stretching mode of the rutile and anatase polymorph modifications of TiO_2 [27]. The FTIR spectra of pure TiO_2 and Fe-doped titania (as shown in Fig. 3) illustrate the absorption peaks at about 1536 cm^{-1}. An absorption band at about 1530 cm^{-1} was noted but not interpreted in [28]. The relative intensity of this band is low for an undoped sample, has a maximum for two-phase crystalline 10Fe sample and decreases for amorphous 20Fe sample. The peak at 1540 cm^{-1} corresponds to the asymmetric vibration of the surface group of COO [29]. At the same time, the close adsorption region at about 1560 cm^{-1} band can be associated with the vibration mode of adsorbed water, and the band frequency depends linearly on the distance between water molecules and the surface of the TiO_2 nanocluster [30]. The difference in the specific surface area of 5Fe and 10Fe samples is relatively small (Fig. 2); therefore, the presence of Fe ions in the surface layers of titania particles changes the adsorption conditions.

One of the reasons is the concentration of oxygen vacancies with increasing Fe^{3+} content, which corresponds to the reduction of the rutile lattice constant with isomorphic substitution of Ti^{4+} ions. Broken Ti–O bonds and distorted coordination octahedron cause the material density increase and the unit cell decrease, as well as the appearance of mechanical stresses [31].

The values of the specific surface area of 5Fe, 10Fe and 20Fe samples are very close, so the difference in the results of thermal analysis (Fig. 4a) cannot be explained by the removal of adsorbed surface species. As shown in Fig. 4b, the shift of the maximum weight loss rate toward lower temperatures from 140 to 110 °C is observed with an increase in the Fe content from 5 to 20 wt. %. The same dynamics has a position of endothermic peaks (Fig. 4c) on the DTA curve taken as the glass transition temperature (157, 144 and 130 °C for 5Fe, 10Fe and 20Fe, respectively) that can be assigned to the crystallization of the amorphous component of materials, accompanied by the removal of adsorbed water molecules and hydroxyl groups. The broad exothermic peaks observed in a range of 400-800 °C correspond to the anatase-rutile transition without weight loss. The material with the maximum content of Fe ions has the maximum thermal stability: for 20Fe samples, the transition temperature is the highest (about 575 °C).

Mossbauer spectra of Fe-doped TiO_2 samples at Fe contents of 5, 10 and 20 wt. % (Fig. 5a) consist of a single doublet component.

The fitting procedures realized for each spectrum allow to determine the parameters of hyperfine interactions (isomer shift δ, quadrupole splitting Δ, line width

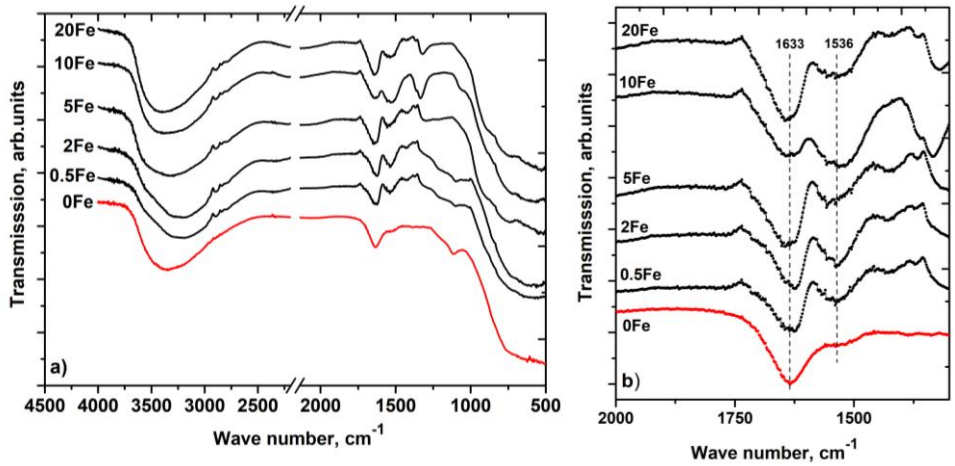

Fig.3 – FTIR spectra of Fe-doped TiO_2 in a range of 500-4000 cm^{-1} (a) and 1300-2000 cm^{-1} (b)

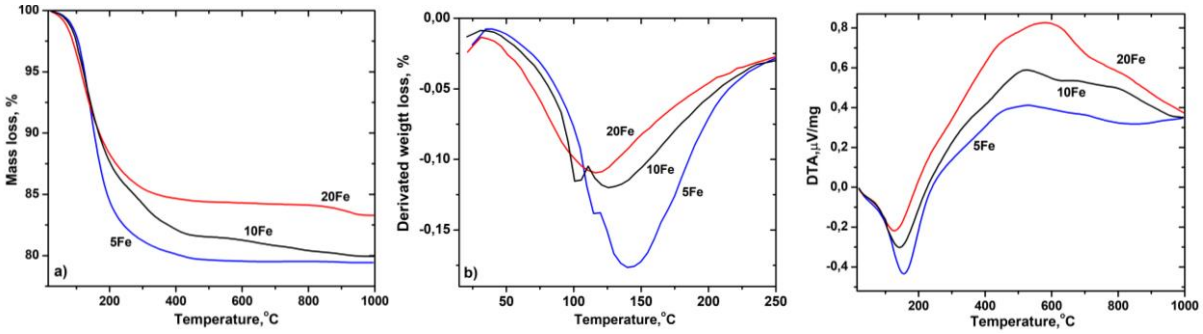

Fig. 4 – TG (a), DTG (b) and DTA (c) curves of Fe-doped TiO_2

ω). All doublets have close isomer shift values (0.55-0.57 mm/s) that is associated with Fe^{3+} ions in a high-spin state in octahedral coordination as a result of isomorphic substitution of Ti^{4+} ions for Fe^{3+} without the presence of an Fe-containing amorphous phase [32].

An increase in the quadrupole splitting values from 0.71 to 0.74 and 0.79 mm/s for 5Fe, 10Fe and 20Fe samples, respectively, corresponds to an increase in the structural disorder. A simultaneous decrease in the line width (in a range of 0.55-0.49 mm/s) is the result of a decrease in the number of non-equivalent crystallographic sites of localization of Fe^{3+} ions with the doping degree enlargement. Isothermal annealing of 20Fe sample was realized in a temperature range of 200-900 °C with a Mossbauer study of the obtained materials (Fig. 5b). Separation of the magnetically ordered phase (about 20-22 % of the integral intensity) was observed after thermal treatment at 500 °C. The quadrupole splitting values of the sextet components for the 20Fe-500 sample correspond to the α-Fe_2O_3 phase (0.21 mm/s), but hyperfine magnetic field B_{hf} (48.5 T) is much lower than expected for this compound (typical values are about 51.2-51.7 T [33, 34]). An increase in the annealing temperature to 700 °C leads to growth of the magnetic ordered component relative intensity to 32 without significant changes in quadrupole splitting and hyperfine magnetic field values.

At the same time, a decrease in the quadrupole splitting and an increase in the line width of the doublet component were observed. A subsequent increase in the annealing temperature causes the disappearance of Fe^{3+} in the magnetically ordered state without changing the doublet component parameters.

An additional XRD study of 20Fe-900 sample shows the formation of Fe-containing pseudobrookite Fe_2TiO_5 phase [35] with a content of about 29 mol. % and transitions of amorphous anatase to monoclinic titania (space group symmetry C12/m1) typically obtained by thermal decomposition of layered $H_2Ti_3O_7$ titanites [36]. The spectra parameters of 20Fe-900 sample are close to the data obtained for the pseudobrookite phase synthesized by the decomposition of $FeCl\{Ti_2(OPri)_9\}$ precursor at 1000 °C [37].

An investigation of the photocatalytic performance of all Fe-containing samples was done. Typical UV-vis absorption spectra of titania-containing (20Fe sample) sol are presented in Fig. 6a. The gradual decrease in the absorption peaks at 665 nm with increasing irradiation time is the result of MB oxidation. The degradation diagrams of the prepared samples for MB (Fig. 6b) allow to calculate the rate values of MB oxidation reactions. It was observed that increasing the Fe content causes an increase in the degradation reaction rate (Fig. 6c).

The reaction rate increases from about 0.008 to 0.028 min^{-1}. A commercial photocatalyst Degussa (Evonic) P25 (anatase content of about 70 wt. %, presence of an amorphous phase, average particle size of about 20 nm [38]) was used for a comparative analysis of the photocatalytic performance of Fe-doped TiO_2. It was determined that the reaction rate of MB photocatalytic degradation with P25 sample under the same experimental conditions is about 0.029 min^{-1}, which is

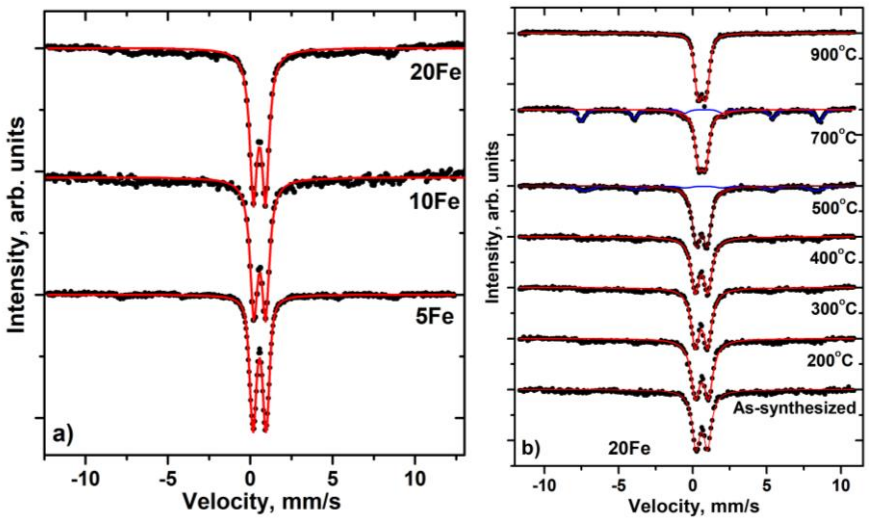

Fig. 5 – Mossbauer data of Fe-doped TiO_2: (a) spectra obtained for samples with different Fe content (5, 10 and 20 wt. %) and (b) spectra obtained for 20Fe sample annealed in a temperature range of 200-900 °C

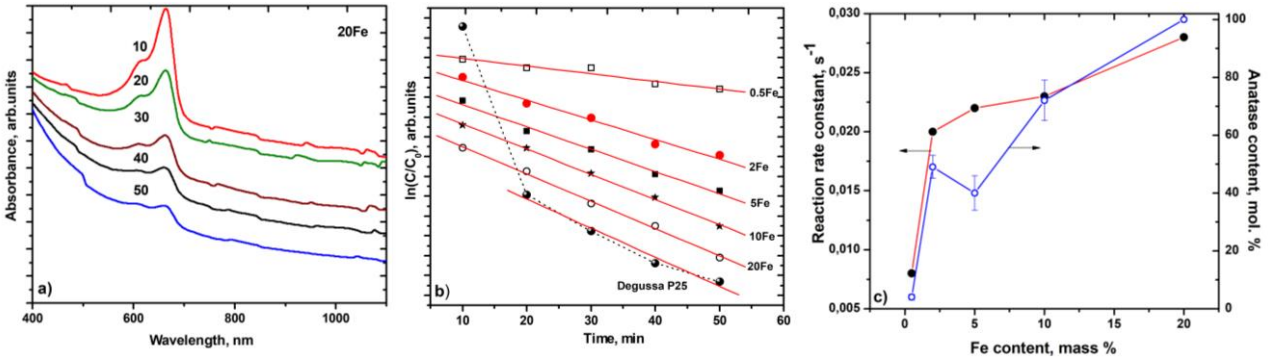

Fig. 6 – Photocatalytic performance of Fe-doped TiO_2 samples:(a) UV-vis absorption spectra changes as a result of photocatalytic degradation time of MB (0.01 g/l) with 20Fe sample (0.1 g/l); (b) the effect of the Fe concentration on the MB degradation diagrams; (c) the reaction rate constant and anatase phase content as a function of Fe concentration in Fe-doped titania

close to the performance of 20Fe sample. A feature of the P25 experiment is a rapid decrease in the absorption of the MB solution at the initial stage of the procedure, which despite the MB solution absorption at the initial stage of procedure that can be explained by the dye adsorption on the P25 titania particles (Fig. 6b). A clear correlation (Pearson coefficient value is about 0.90-0.91) was observed between the reaction rate constant of MB oxidation and the relative content of the anatase phase in catalysts (Fig. 6c). It was supposed that amorphous 20Fe sample consists of ultrafine anatase only. As a result, the catalyst phase composition is more important than the formation of oxygen vacancies due to the substitution of Fe^{3+} for Ti^{4+} ions in the titania lattice, which can promote the formation of oxygen vacancies, dissociation of H_2O, and an increase in the concentration of surface hydroxyl groups [39]. This assumption is confirmed by the stability of the position of the absorption band edges for all Fe-containing samples without a remarkable shift to the visible range with increasing Fe content, as was observed in [40].

4. CONCLUSIONS

The variation of the Fe content in Fe-doped titania, obtained by sol-gel synthesis based on the conventional hydrolysis of titanium tetrachloride and ferric chloride hexahydrate, makes it possible to control both the anatase phase content and the degree of crystallinity of the obtained TiO_2. The absence of an Fe-containing phase and the stability of the position of the absorption band edges were observed for Fe-doped titania samples with a Fe content of up to 20 wt. %. The observed specific surface area of Fe-doped titania linear growth in a range of 70-350 m^2/g with an increase in the iron content in the range of 0-5 mass % can be caused by the formation of anion vacancies due to the substitution of Fe^{3+} ions into the titania matrix. Isothermal annealing of Fe-doped titania at 900 °C causes the formation of pseudobrookite and monoclinic TiO_2 phases. The photocatalytic activity of Fe-doped TiO_2 with an Fe content of 20 wt. % in the photodegradation reaction of methylene blue dye at a wavelength of 365 nm is close to the Degussa P25 characteristics.

REFERENCES

1. H.M. Yadav, J.S. Kim, J.S. Pawar, *Korean J. Chem. Eng.* **33** No 7, 1989 (2016).
2. Z. Li, Z. Yao, A.A. Haidry, T. Plecenik, L. Xie, L. Sun, Q. Fatima, *Int. J. Hydrogen Energy* **43** 21114 (2018).
3. V. Aravindan, Y.S. Lee, R. Yazami, S. Madhavi, *Mater. Today* **18** No 6, 345 (2015).
4. A.J. Frank, N. Kopidakis, J. Van De Lagemaat, *Coordin. Chem. Rev.* **248** No 14-15, 1165 (2004).
5. Y. Wang, Y. He, Q. Lai, M. Fan, *J. Environ. Sci.* **26** No 11, 2139 (2014).
6. A. Zaleska, *Recent Patents on Engineering* **2** No 3, 157 (2008).
7. Y. Shen, T. Xiong, T. Li, K. Yang, *Appl. Catal. B-Environ.* **83** No 3-4, 177 (2008).
8. Y. Zhang, Y. Shen, F. Gu, M. Wu, Y. Xie, J. Zhang, *Appl. Surf. Sci.* **256** No 1, 85 (2009).
9. J. Zhu, W. Zheng, B. He, J. Zhang, M. Anpo, *J. Mol. Catal. A-Chem.* **216** No 1, 35 (2004).
10. I. Ganesh, P.P. Kumar, A.K. Gupta, P.S. Sekhar, K. Radha, G. Padmanabham, G. Sundararajan, *Proc. Appl. Ceram.* **6** No 1, 21 (2012).
11. V.O. Kotsyubynsky, I.F. Myronyuk, L.I. Myronyuk, V.L. Chelyadyn, M.H. Mizilevska, A.B. Hrubiak, F.M. Nizamutdinov, *Materialwiss Werkst.* **47** No 2-3 288 (2016).
12. J. Rodriguez-Carvajal, *Newsletter* **26**, 12 (2001).
13. T.E. Weirich, M. Winterer, S. Seifried, H. Hahn, H. Fuess, *Ultramicroscopy* **81** No 3-4, 263 (2000).
14. T.M. Sabine, C.J. Howard, *Acta Crystall.* **B38**, 701 (1982).
15. Y. Wang, H. Cheng, Y. Hao, J. Ma, W. Li, S. Cai, *J. Mater. Sci.* **34** No 15, 3721 (1999).
16. V.O. Kotsyubynsky, I.F. Myronyuk, V.L. Chelyadyn, A.B. Hrubiak, V.V. Moklyak, S.V. Fedorchenko, *Nanoscale Res. Lett.* **12** No 1, 1 (2017).
17. L. Forro, O. Chauvet, D. Emin, L. Zuppiroli, H. Berger, F. Levy, *J. Appl. Phys.* **75** No 1, 633 (1994).
18. H. Yin, Y. Wada, T. Kitamura, S. Kambe, S. Murasawa, H. Mori, S. Yanagida, *J. Mater. Chem.* **11**, 1694 (2001).
19. R.D. Shannon, J.A. Pask, *J. Am. Ceram. Soc.* **48** No 8, 391 (1965).
20. N. S. Vujicic, M. Gotic, S. Music, M. Ivanda, S. Popovic, *J. Sol-Gel Sci. Technol.* **30** No 1, 5 (2004).
21. M. Kang, S.J. Choung, J.Y. Park, *Catal. Today.* **87** No 1-4, 87 (2003).
22. Y.-H. Zhang, A. Reller, *J. Mater. Chem.* **11** No 10, 2537 (2001).
23. M.Q. Cao, K.Liu, H.M. Zhou, H.M. Li, X.H. Gao, X.Q. Qiu, M. Liu, *J. Cent. South Univ. T.* **26** No 6, 1503 (2019).
24. A. Navrotsky, *Geochem. Trans.* **4**, 34 (2003).
25. M. Crisan, A. Jitianu, D. Crisan, M. Balasoiu, N. Dragan, M. Zaharescu, *J. Optoelectron. Adv. Mater.* **2** No 4, 339 (2000).
26. M. Crisan, A. Jitianu, D. Crisan, M. Balasoiu, N. Dragan, M. Zaharescu, *J. Mater. Chem.* **15**, 1263 (2005).
27. R.S. Devi, D.R. Venckatesh, D.R. Sivaraj, *Int. J. Innov. Res. Sci. Eng. Technol.* **3**, 15206 (2014).
28. J.B. Yin, X.P. Zhao, *Chem. Mater.* **14** No 11, 4633 (2002).
29. T. Theophile, *Infrared Spectroscopy: Materials Science, Engineering and Technology* (London: BoD–Books on Demand: 2012).
30. R. Kevorkyants, A.V. Rudakova, Y.V. Chizhov, K.M. Bulanin, *Chem. Phys. Lett.* **662**, 97 (2016).
31. Y. Liu, C.Y. Liu, Q.H. Rong, Z. Zhang, *Appl. Surf. Sci.* **220** No 1-4, 7 (2003).
32. E. Kuzmann, S. Nagy, A. Vertes, *Pure Appl. Chem.* **75**, 801 (2003).
33. I.S. Lyubutin, C.R. Lin, Y.V. Korzhetskiy, T.V. Dmitrieva, R.K. Chiang, *J. Appl. Phys.* **106** No 6, 034311 (2009).
34. V.O. Kotsyubynsky, V.V. Mokliak, A.B. Grubiak, P.I. Kolkovsky, A.S.A.H. Zamil, *J. Nano- Electron. Phys.* **5** No 1, 01024 (2013).
35. H.D. Ngo, T.D. Ngo, A. Tamanai, K. Chen, N.T. Cuong, O.S. Handegard, T. Nagao, *Cryst. Eng. Comm.* **21**, 34 (2019).
36. T.P. Feist, P.R Davies, *J. Solid. State Chem.* **101** No 2, 275 (1992).
37. P.H.C. Camargo, G.G. Nunes, G.R. Friedermann, D.J. Evans, G.J. Leigh, G. Tremiliosi-Filho, E.L. de Sa, A.G. Zarbin, J.F. Soares, *Mater. Res. Bull.* **38**, 1915 (2003).
38. B. Ohtani, O.O. Prieto-Mahaney, D. Li, R. Abe, *J. Photoch. Photobio. A.* **216** No 2-3, 179 (2010).
39. Y. Yang, H. Zhong, C. Tian, Z. Jiang, *Surface Sci.* **605** No 13-14, 1281 (2011).

Оксид титану, легований залізом: синтез, структурні, магнітні та фотокаталітичні властивості

Іван Миронюк[1], Володимир Коцюбинський[1], Ігор Микитин[1], Юлія Коцюбинська[2], Володимира Бойчук[1], Василь Федорів[1]

[1] *ДВНЗ «Прикарпатський національний університет імені Василя Стефаника», вул. Шевченка, 57, 76018 Івано-Франківськ, Україна*

[2] *Івано-Франківський національний медичний університет, вул. Галицька, 2, 76018 Івано-Франківськ, Україна*

Вплив масової концентрації іонів Fe^{3+} на фазовий склад та морфологію допованого залізом діоксиду титану (Fe:TiO_2), отриманого методом двостадійного гідролізу $TiCl_4$ та $FeCl_3{\cdot}6H_2O$ при фінальному pH = 3.5, досліджувався методами XRD, FTIR, Месбауерівської спектроскопії, термічного аналізу та низькотемпературної адсорбції азоту. Збільшення вмісту іонів Fe^{3+} в діапазоні 0-10 мас. % викликає ріст вмісту фази анатазу від 0 до 85-90 %. Середній розмір частинок анатазу зменшується з 31 нм при вмісті заліза 0,5 мас. % до приблизно 4 нм для вмісту заліза 10 мас. %. Матеріал, синтезований при концентрації іонів заліза 20 мас. %, аморфний (дані XRD) без присутності магнітовпорядкованих залізовмісних фаз. Месбауерівські спектри всіх зразків Fe:TiO_2 формуються тільки дублетною компонентою зі значеннями ізомерного зсуву 0,55-0,57 мм/с, що відповідає Fe^{3+} у високоспіновому стані в октаедрічній координації, тому високоймовірним є ізоморфне заміщення іонів Ti^{4+} на Fe^{3+} в кристалічних гратках анатазу та рутилу. Відпал зразка Fe:TiO_2 з максимальним ступенем допування (20 мас. %) при температурі 900 °C призводить до утворення фази псевдобрукіту Fe_2TiO_5 та переходу аморфного анатазу в моноклінний діоксид титану (просторова група симетрії C12/m1). Спостерігається лінійний ріст питомої площі поверхні (BET) Fe:TiO_2 з 70 до 350 м^2/г при збільшенні вмісту іонів заліза від 0 до 5 мас. %; подальше збільшення вмісту іонів заліза не впливає на значення питомої площі поверхні

матеріалів. Зростання концентрації кисневих вакансій зі збільшенням вмісту Fe^{3+}, спостережуване методом FTIR, відповідає зниженню величин сталої гратки фаз анатазу та рутилу. Температура фазового переходу анатаз-рутил (дані термічного аналізу) найвища (близько 575 °C) для матеріалу з максимальним вмістом іонів Fe. Фотокаталітична активність допованих Fe зразків TiO_2, досліджувана на прикладі реакції деградації метиленового синього, зростає зі збільшенням вмісту іонів Fe, корелюючи з відносним вмістом фази анатазу. Константа реакції фотодеградації при застосуванні Fe:TiO_2 зростає від 0,008 до 0,028 $хв^{-1}$, в той час як аналогічний параметр при застосуванні в тих же експериментальних умовах комерційного фотокаталізатора Degussa P25 становить 0,029 $хв^{-1}$.

Ключові слова: Оксид титану, легований залізом, Гідроліз, Поліконденсація, Нуклеація, Оксид титану.